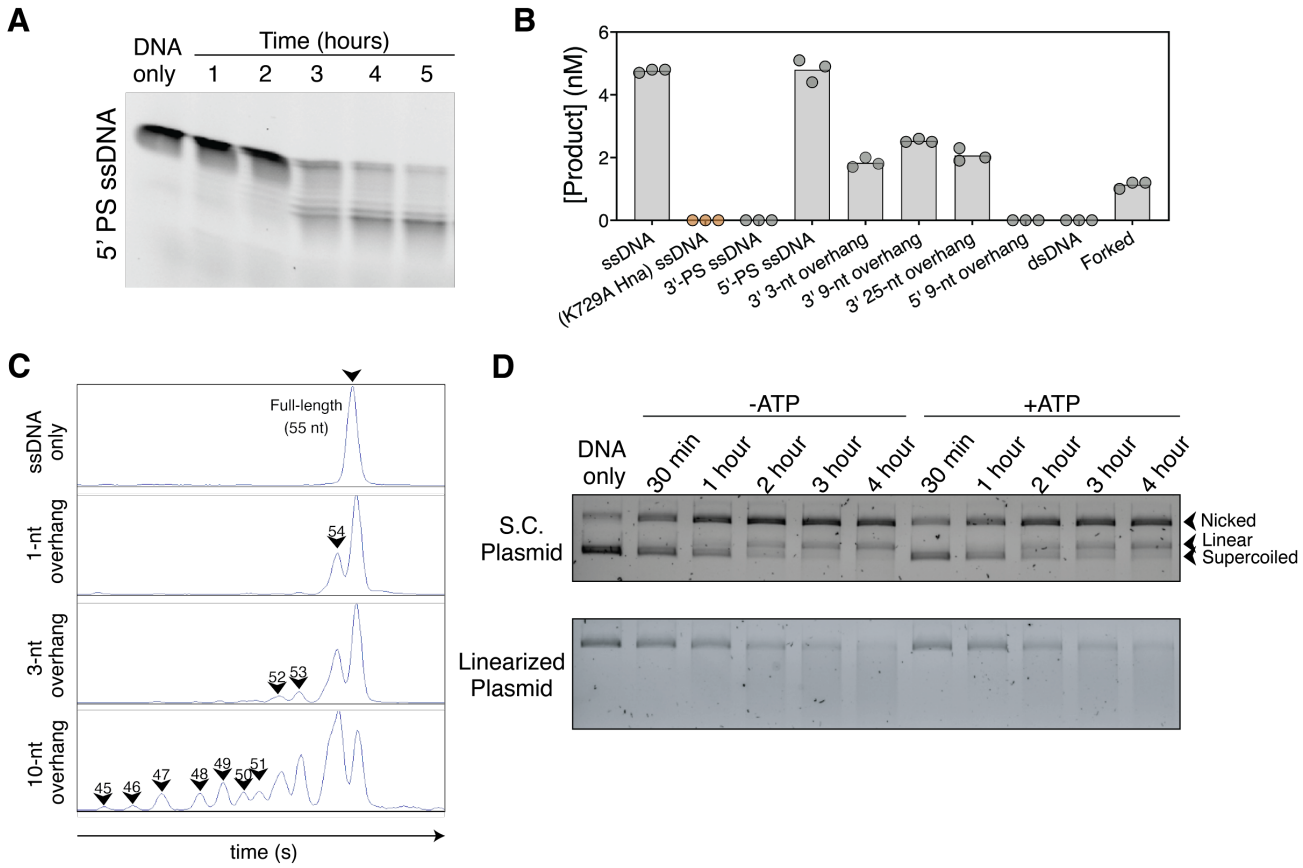

Supplementary Fig. 1 | Hna degrades single-stranded and plasmid DNA. A, Exonuclease activity over time using ssDNA with a series of 5'-phosphorothioate (PS) modifications showing unperturbed cleavage. Gel is representative of 3 independent experiments. **B,** Quantification of DNA cleavage by Hna in the presence of various substrates using capillary electrophoresis. Data represents product formation across three independent, biological replicates. **C,** Raw fluorescence peaks corresponding to differently sized fluorescently-labeled cleavage products. DNA only negative control (55 nucleotides) shown at the top. **D,** Time course Hna cleavage using supercoiled (S.C.) and linearized plasmid in the presence or absence of ATP. Distinct species of DNA are denoted on the right. Gel is representative of 4 independent experiments. Source data are provided as a Source Data file.

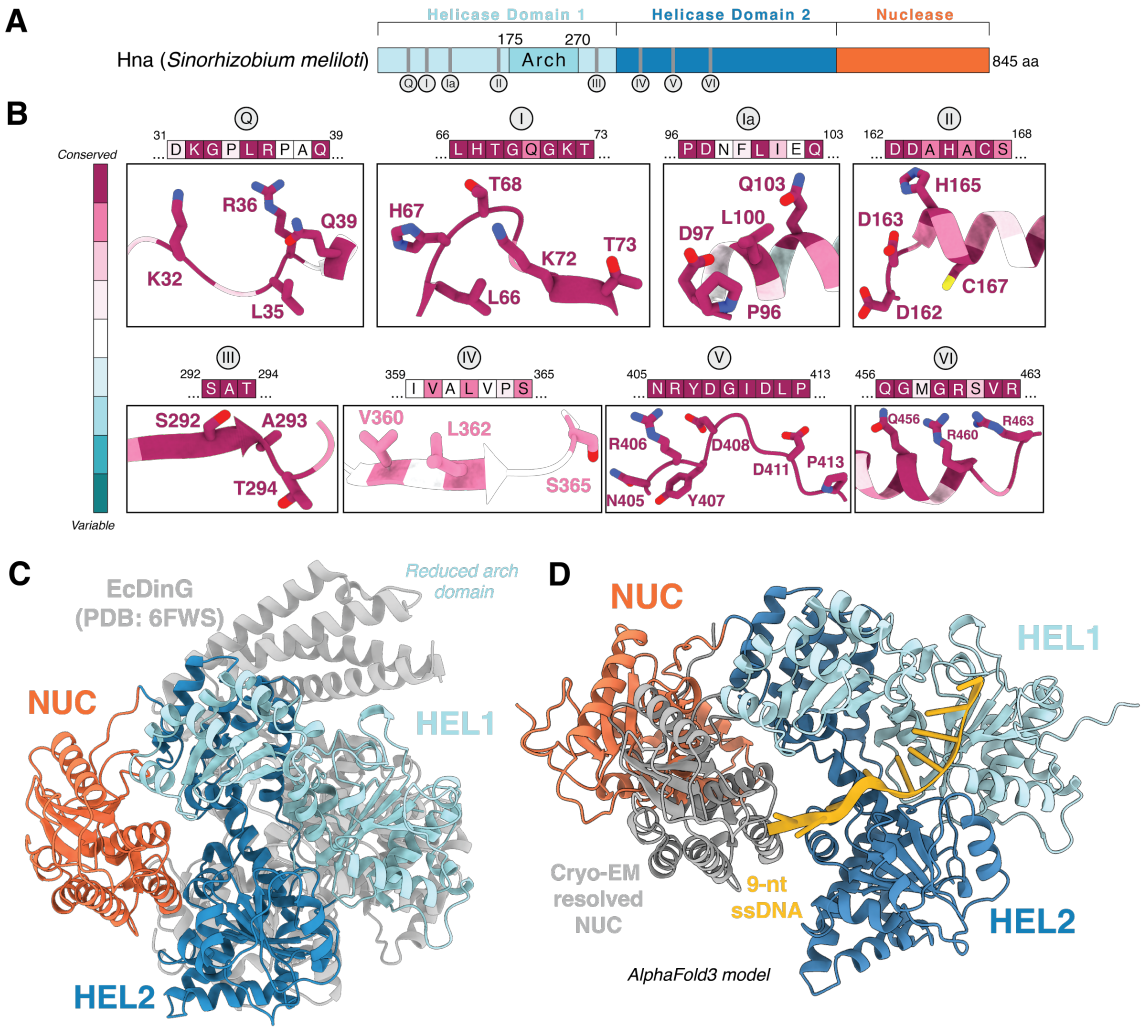

Supplementary Fig. 2 | Hna structural motifs and conservation. A, Domain organization of Hna from *S. meliloti*. The two helicase modules and C-terminal nuclease domain are shown in blue and orange, respectively. Canonical HEL1 and HEL2 functional motifs are labeled, as well as the HEL1 Arch domain. **B,** Magnified view of each identified SF2 helicase motif. Residues are colored by conservation with position and sequence listed above. **C,** Overlay of determined Hna monomer structure (colored) and structurally similar protein, *EcDinG* (PDB: 6FWS; gray). Hna and DinG helicase domains are highly similar with notably reduced Arch domain in Hna. **D,** AlphaFold3 prediction of Hna bound to a 9-nucleotide ssDNA substrate (colored) overlaid with the NUC domain of Hna monomer structure (gray). The predicted substrate fully occupies the Hna DNA binding site and promotes a unique NUC domain rearrangement.

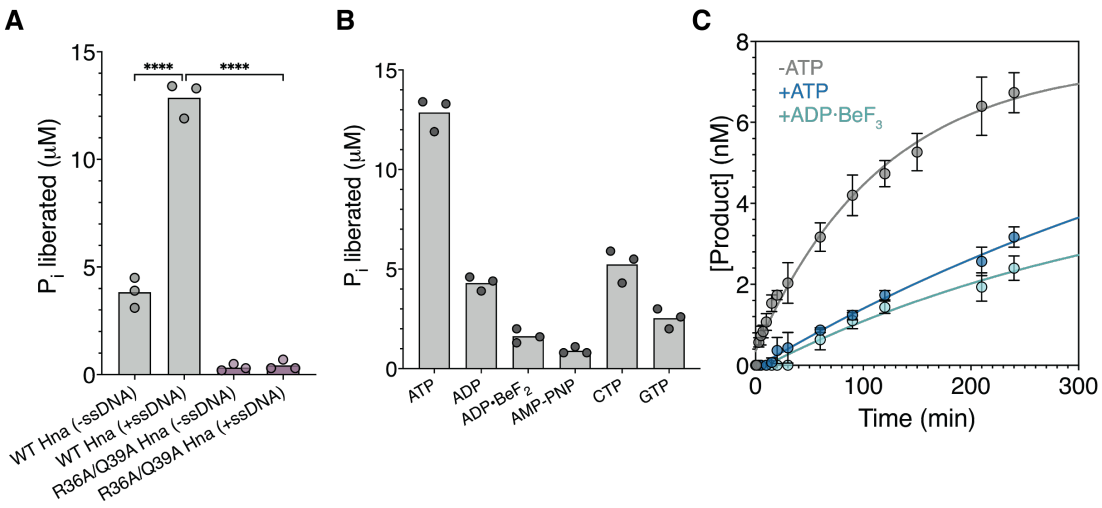

Supplementary Fig. 3 | Hna exhibits ssDNA-stimulated ATPase activity. A, Malachite green ATPase assay using wild-type Hna or ATP-binding mutant (R36A/Q39A) with and without ssDNA present (n=3 independent, biological replicates). Phosphate concentration was determined after 30 minutes of incubation. Statistical significance is evaluated via one-way ANOVA; *$p < 0.05$, **$p < 0.01$, ***$p < 0.001$. **B,** Malachite green phosphate detection assay using wild-type Hna with ssDNA present and various nucleotide analogs. Phosphate concentration was determined after 30 minutes of incubation (n=3 independent, biological replicates). **C,** Quantification of ssDNA cleavage by Hna in the presence and absence of ATP or ADP·BeF_3 using capillary electrophoresis. Data shown are the mean ± standard deviation of three independent experiments for each condition. Source data are provided as a Source Data file.

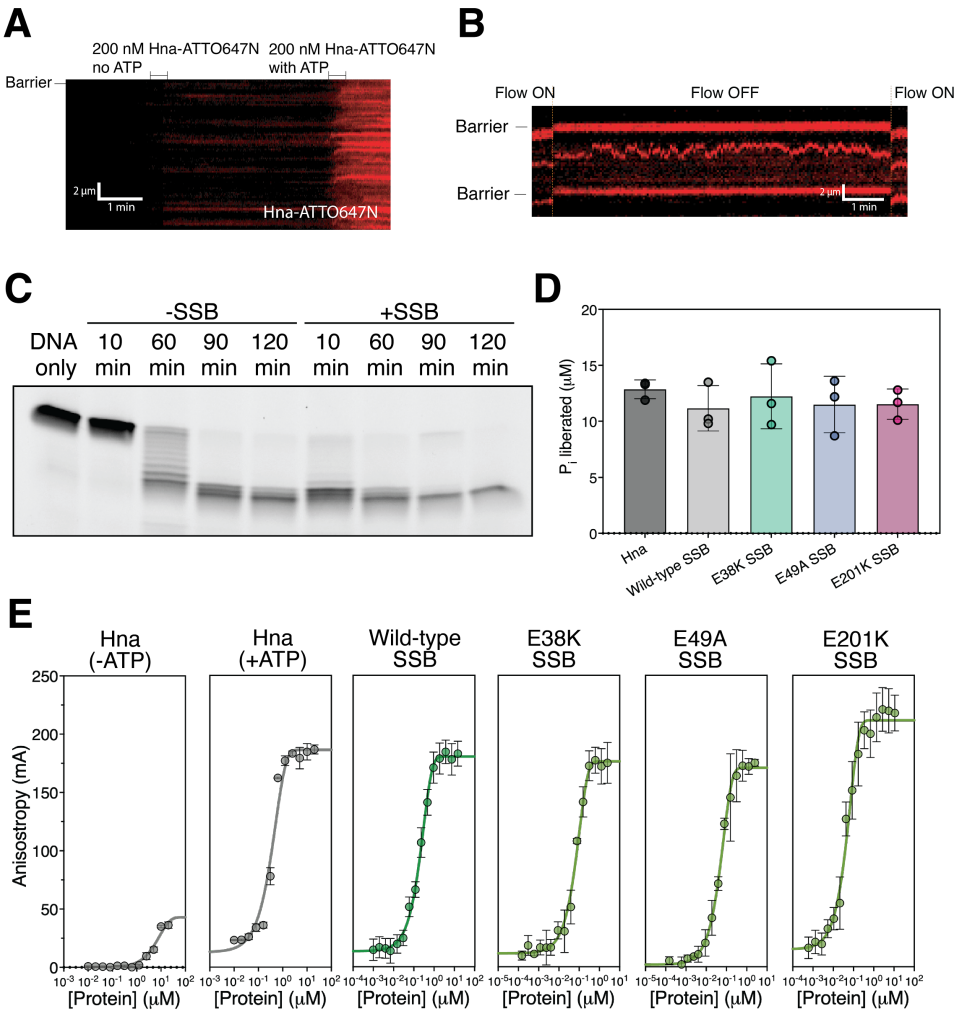

Supplementary Fig. 4 | Hna is an ATP-dependent DNA binding protein. A, Representative kymograph showing ATP-dependent binding of ssDNA by Hna (red). ATP was injected at the time indicated on the kymograph promoting increased binding events. **B,** Representative kymograph showing passive diffusion of Hna (red) along ssDNA in the absence of buffer flow. **C,** Time course cleavage of ssDNA by Hna in the absence or presence of phage-encoded 5A SSB. **D,** Malachite green ATPase assay using wild-type Hna only (Hna) or combined with various SSB mutants with single-stranded DNA present. Phosphate concentration was determined after 30 minutes of incubation 37°C. Data shown are the mean ± standard deviation of three independent, biological replicates for each condition. **E,** Hna and 5A SSB binding curves after incubation with fluorescently labeled ssDNA. Data shown are the mean ± standard deviation of three independent, biological replicates fit to a one-phase decay function. Source data are provided as a Source Data file.

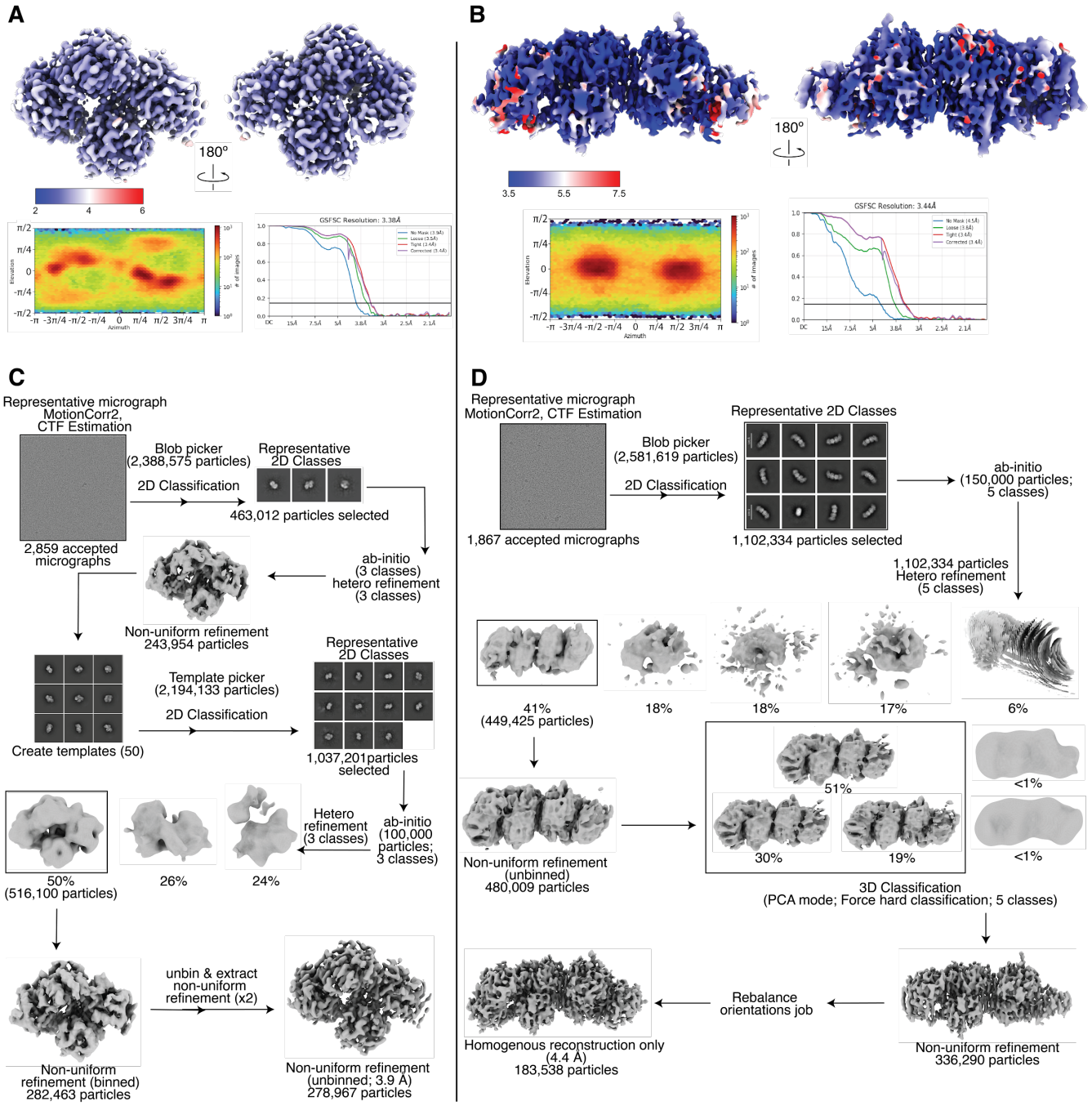

Supplementary Fig. 5 | Structural analysis of Hna. A, Unsharpened maps colored by local resolution (top) for Hna monomer and **B,** Hna dimer. Accompanying gold-standard FSC curves for cryo-EM reconstructions (left) with Euler diagrams showing orientation distributions of cryo-EM reconstructions (right). Resolutions were estimated at FSC=0.143. **C,** Data processing pipelines for Hna monomer and **D,** Hna dimer.

Supplementary Table 1 | List of DNA sequences used in this study.

Oligo Name	Sequence (5' to 3')
ssDNA (55-nt)	agctgacgtttgtatgtctgcgtctcatctttatgcgtcagcagagatttctgct
dsDNA complement	agcagaaatctctgctgacgcataaagatgagacgcagacatacaaacgtcagct
3' 1-base overhang complement	gcagaaatctctgctgacgcataaagatgagacgcagacatacaaacgtcagct
3' 3-base overhang complement	agaaatctctgctgacgcataaagatgagacgcagacatacaaacgtcagct
3' 9-base overhang complement	ctctgctgacgcataaagatgagacgcagacatacaaacgtcagct
3' 10-base overhang complement	tctgctgacgcataaagatgagacgcagacatacaaacgtcagct
3' 25-base overhang complement	agatgagacgcagacatacaaacgtcagct
5' 9-base overhang complement	agcagaaatctctgctgacgcataaagatgagacgcagacatacaa
Forked complement	tgagacgcagacatacaaacgtcagcttgagacgcagacatacaaacgtcagct

Supplementary Table 2 | Cryo-EM data collection, refinement, and validations statistics.

	Hna Monomer (EMD-75470; PDB 10UJ)	Hna Dimer (EMD-73047; PDB 9YKJ)
Data Collection and Processing		
Voltage (kV)	200	200
Electron exposure (e-/Å^2)	49	49
Defocus range (μm)	-1.5 to -2.5	-1.5 to -2.5
Pixel size (Å)	0.94	0.94
Symmetry imposed	C1	C1
Initial particle images (no.)	2,194,133	2,581,619
Final particle images (no.)	278,967	185,538
Map resolution (Å)	3.9	4.4
FSC threshold	0.143	0.143
Refinement		
Initial model used (PDB code)	AlphaFold3	AlphaFold3
Model resolution (Å)	3.8	3.7
FSC threshold	0.5	0.5
Map sharpening B factor (Å^2)	167.3	121.9
Model composition		
Non-hydrogen atoms	6490	5952
Protein residues	821	1205
Nucleotides	0	0
R.m.s deviations		
Bond lengths (Å)	0.004	0.003
Bond angles (°)	0.808	0.819
Validation		
MolProbity score	1.2	1.18
Clashscore	3.93	0.57
Poor rotamers (%)	0	0
Ramachandran plot		
Favored (%)	97.92	92.03
Allowed (%)	2.08	7.29
Disallowed (%)	0	0